

Article

Lévy Femtoscopy with PHENIX at RHIC

Máté Csanád  for the PHENIX Collaboration

Eötvös Loránd University, H-1117 Budapest, Pázmány P. s. 1/A, Hungary

* Correspondence: csanad@elte.hu; Tel.: +36-1-411-6500

Abstract: In this paper we present the measurement of charged pion two-particle femtoscopy correlation functions in $\sqrt{s_{NN}} = 200$ GeV Au+Au collisions, in 31 average transverse mass bins, separately for positive and negative pion pairs. Lévy-shaped source distributions yield a statistically acceptable description of the measured correlation functions, with three physical parameters: correlation strength parameter λ , Lévy index α and Lévy scale parameter R . The transverse mass dependence of these Lévy parameters is then investigated. Their physical interpretation is also discussed, and the appearance of a new scaling variable is observed.

Keywords: RHIC; PHENIX; femtoscopy; Bose-Einstein correlations; Lévy distribution; anomalous diffusion; critical point; in-medium mass modification

1. Introduction

In nucleus-nucleus collisions at the Relativistic Heavy Ion Collider, a strongly coupled Quark Gluon Plasma (sQGP) is formed [1–4], creating hadrons at the freeze-out. The measurement of femtoscopy correlation functions is used to infer the space-time extent of hadron creation. The field of femtoscopy was founded by the astronomical measurements of R. Hanbury Brown and R. Q. Twiss [5] and the high energy physics measurements of G. Goldhaber and collaborators [6,7]. If interactions between the created hadrons, higher order correlations, decays and all other dynamical two-particle correlations may be neglected, then the two-particle Bose-Einstein correlation function is simply related to the source function $S(x, k)$ (which describes the probability density of particle creation at the space-time point p and with four-momentum x). This can be understood if one defines $N_1(p)$ as the invariant momentum distribution and $N_2(p_1, p_2)$ as the momentum pair distribution. Then the definition of the correlation function is [8]:

$$C_2(p_1, p_2) = \frac{N_2(p_1, p_2)}{N_1(p_1)N_1(p_2)}, \text{ where} \quad (1)$$

$$N_2(p_1, p_2) = \int S(x_1, p_1)S(x_2, p_2)|\Psi_2(x_1, x_2)|^2 d^4x_1 d^4x_2. \quad (2)$$

Here $\Psi_2(x_1, x_2)$ is two-particle wave function, for which

$$|\Psi_2(x_1, x_2)|^2 = \left| \Psi_2^{(0)}(x_1, x_2) \right|^2 = 1 + \cos [(p_1 - p_2)(x_1 - x_2)] \quad (3)$$

follows in an interaction-free case, denoted by the superscript ⁽⁰⁾. This leads to

$$C_2^{(0)}(Q, K) \simeq 1 + \left| \frac{\tilde{S}(Q, K)}{\tilde{S}(0, K)} \right|^2, \text{ where} \quad (4)$$

$$\tilde{S}(Q, K) = \int S(x, K)e^{iQx} d^4x \text{ is the Fourier-transformed of } S, \quad (5)$$

24 and $Q = p_1 - p_2$ is the momentum difference, $K = (p_1 + p_2)/2$ is the average momentum, and we
 25 assumed, that $Q \ll K$ holds for the investigated kinematic range. Usually, correlation functions
 26 are measured versus Q , for a well-defined K -range, and then properties of the correlation functions
 27 are analyzed as a function of the average K of each range. If the source is a static Gaussian with a
 28 radius R , then the correlation function will also be a Gaussian with an inverse radius, hence it can be
 29 described by one plus a Gaussian: $1 + \exp(-(QR)^2)$. However, if the source is expanding, then the
 30 observed Gaussian radius R does not represent the geometrical size, but rather a length of homogeneity,
 31 depending on the average momentum K . The approximate dependence of $R^{-2} \propto A + Bm_T$ is observed
 32 for various collision systems, collision energies and particle types [9,10], where $m_T = \sqrt{K_T^2 + m^2c^2}$,
 33 and K_T is the transverse component of K . This can be interpreted as a consequence of hydrodynamical
 34 expansion [11,12]. See Ref. [13] (and references therein) for details.

35 Usually, the shape of the particle emitting source is assumed to be Gaussian, however, this does
 36 not seem to be the case experimentally [14,15]. In an expanding hadron resonance gas, increasing mean
 37 free paths lead to a Lévy-flight, anomalous diffusion, and hence to spatial Lévy distributions [16–18].
 38 The one-sided, symmetric Lévy distribution as a function of spatial coordinate r is defined as:

$$\mathcal{L}(\alpha, R, r) = (2\pi)^{-3} \int d^3q e^{iqr} e^{-\frac{1}{2}|qr|^\alpha}, \quad (6)$$

39 where α is the Lévy index and R is the Lévy scale. Then $\alpha = 2$ gives back the Gaussian case and $\alpha = 1$
 40 yields a Cauchy distribution. This source function leads to a correlation function of

$$C_2(Q, K) = 1 + e^{-(Q \cdot R(K))^\alpha}. \quad (7)$$

41 It is interesting to observe that the spatial Lévy distribution results in power-law tails in the spatial
 42 correlation function, with an exponent of $-1 - \alpha$. Such power-law spatial correlations are also expected
 43 in case of critical behavior, with an exponent of $-(d - 2 + \eta)$, with η being the critical exponent. It is
 44 easy to see that in this case, $\eta = \alpha$, i.e. the Lévy exponent is identical to the critical exponent η [19].
 45 The second order QCD phase transition is expected to be in the same universality class as the phase
 46 transition of the 3D Ising model or the random field 3D Ising model (see Refs [20–23] for details
 47 and values for the critical exponents), and hence around the critical point, $\alpha \leq 0.5$ values may be
 48 expected [19]. Since the exploration of the QCD phase diagram, in particular the search for the QCD
 49 critical endpoint is one of the major goals of experimental heavy ion physics nowadays, the above
 50 discussed relations yield additional motivation for the measurement and analysis of Bose-Einstein
 51 correlation functions.

52 Furthermore, it is important to note, that not all pions are primordial, i.e. not all of them are created
 53 directly from the collision. A significant fraction of pions are secondary, coming from decays. Hence the
 54 source will have two components: a core of primordial pions, stemming from the hydrodynamically
 55 expanding sQGP (and the decays of very short lived resonances, with half-lives less than a few fm/c),
 56 and a halo, consisting of the decay products of long lived resonances (such as $\eta, \eta', K_S^0, \omega$)

$$S = S_{\text{core}} + S_{\text{halo}}. \quad (8)$$

57 These two components have characteristically different sizes ($\lesssim 10$ fm for the core, > 50 fm for the
 58 halo, based on the half-lives of the above mentioned resonances). In particular, the halo component is
 59 so narrow in momentum-space, that it cannot be resolved experimentally. This leads to

$$\begin{aligned}
 C_2^{(0)}(Q, K) &= 1 + \frac{|\tilde{S}(Q, K)|^2}{|\tilde{S}(0, K)|^2} \simeq 1 + \left(\frac{N_{\text{core}}(K)}{N_{\text{core}}(K) + N_{\text{halo}}(K)} \right)^2 \frac{|\tilde{S}_{\text{core}}(Q, K)|^2}{|\tilde{S}_{\text{core}}(0, K)|^2} \\
 &= 1 + \lambda(K) \frac{|\tilde{S}_{\text{core}}(Q, K)|^2}{|\tilde{S}_{\text{core}}(0, K)|^2}
 \end{aligned} \tag{9}$$

60 where $N_{\text{core}}(K) = \int S_{\text{core}}(Q, K) dQ$ and $N_{\text{halo}}(K) = \int S_{\text{halo}}(Q, K) dQ$ were introduced. Furthermore

$$\lambda(K) = \left(\frac{N_{\text{core}}(K)}{(N_{\text{core}}(K) + N_{\text{halo}}(K))} \right)^2, \tag{10}$$

61 was defined, equivalent to the “intercept” of the correlation function, i.e. its extrapolated value based
62 on the observable Q region:

$$\lim_{Q \rightarrow 0} C_2^{(0)}(Q, K) = 1 + \lambda(K). \tag{11}$$

63 Hence, in the core-halo picture, $\lambda(K)$ is related to the fraction of primordial (core) pions among all
64 (core plus halo) pions at a given momentum. One of the motivations for measuring λ is that it is
65 related [24] to the η' meson yield, expected [25] to increase in case of chiral $U_A(1)$ symmetry restoration
66 in heavy-ion collisions (due to the expected in-medium mass decrease of the η').

67 We also have to take into account that the interaction-free case is not valid for the usual
68 measurement of charged particle pairs, the electromagnetic and strong interactions distort the above
69 simple picture. For identical charged pions, the Coulomb interaction is the most important, and this
70 decreases the number of particle pairs at low momentum differences. This can be taken into account
71 by utilizing the $\Psi_2^{(C)}(x_1, x_2)$ pair wave function solving the Schrödinger-equation for charged particles,
72 given for example in Ref. [13]. With this, a so-called “Coulomb-correction” can be calculated as

$$K_2(Q, K) = \frac{\int d^4x_1 d^4x_2 S(x_1, K - Q/2) S(x_2, K + Q/2) |\Psi^{(C)}(x_1, x_2)|^2}{\int d^4x_1 d^4x_2 S(x_1, K - Q/2) S(x_2, K + Q/2) |\Psi^{(0)}(x_1, x_2)|^2}, \tag{12}$$

73 hence the measured correlation function, including the Coulomb interaction, can be described by

$$C_2^{\text{Coul}}(Q, K) = K_2(Q, K) C_2^{(0)}(Q, K). \tag{13}$$

74 For details, see again Ref. [13] and references therein.

75 In the following, we utilize a generalization of the usual Gaussian shape of the Bose-Einstein
76 correlations, namely we analyze our data using Lévy stable source distributions. We have carefully
77 tested that this source model is in agreement with our data in all the transverse momentum regions
78 reported here: all the Lévy fits were statistically acceptable, as discussed also later. We note that using
79 the method of Lévy expansion of the correlation functions [26], we have found that within errors all
80 the terms that measure deviations from the Lévy shape are consistent with zero. Hence we restrict the
81 presentation of our results to the analysis of the correlation functions in terms of Lévy stable source
82 distributions.

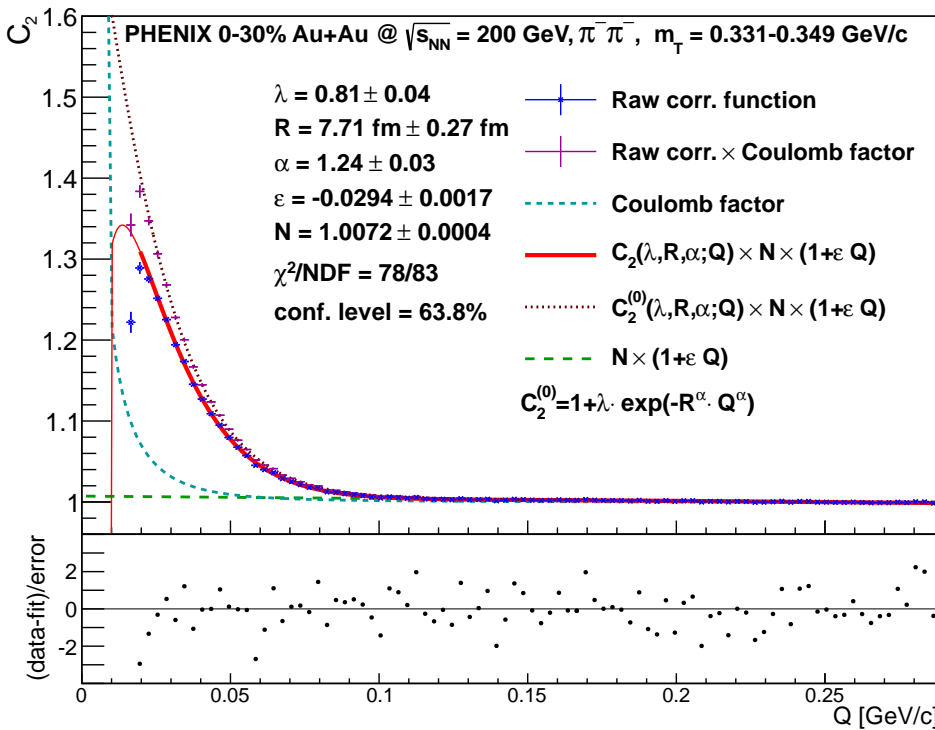


Figure 1. Example fit of $\pi^-\pi^-$ pairs with m_T between 0.331 and 0.349 GeV/c (corresponding to $K_T \in [0.3, 0.32]$ GeV/c), measured in the longitudinal co-moving frame. The fit shows the measured correlation function and the complete fit function, while a “Coulomb-corrected” fit function $C^{(0)}(k)$ is also shown, with the data multiplied by $C^{(0)}/C^{\text{Coul}}$.

83 2. Results

84 We analyzed 2.2 billion 0–30% centrality $\sqrt{s_{NN}} = 200$ GeV Au+Au collisions recorded by the
 85 PHENIX experiment in the 2010 running period.¹ We measured two-particle correlation functions
 86 of $\pi^-\pi^-$ and $\pi^+\pi^+$ pairs, in 31 m_T bins ranging from 228 to 871 MeV, as detailed in Ref. [13]. The
 87 calculated correlation functions based on Lévy-shaped sources gave statistically acceptable descriptions
 88 of all measured correlation functions (all transverse momenta and both charges), see for example Fig. 1.
 89 Note that besides the event selection and the track selection criteria discussed in Ref. [13], we applied
 90 two-track cuts as well, to remove merged tracks and “ghost” tracks, both of which appear due to
 91 the spatial two-track resolution of our tracking system. This removes the very small Q part of the
 92 correlation functions, as seen in Fig 1. A reminiscence of this is seen from the lowest Q point in Fig. 1:
 93 this defines our fit range. The effect of the choice of the fit range and the two-track cuts was studied and
 94 incorporated into the systematic uncertainties. See more details about this topic also in Ref. [13]. The
 95 fact that the correlation functions were described by Lévy fits allows us to study and interpret the m_T
 96 dependence of the fit parameters R , α and λ , as they do represent the measured correlation functions.

97 Let us turn to the resulting fit parameters and their m_T dependence. Parameters λ , R and α
 98 are shown in Fig. 2, as a function of pair m_T (corresponding to the given K_T bin). The detailed
 99 description of the systematic uncertainties is given in Ref. [13], here we focus on the characteristics of
 100 the m_T dependencies. In the top left panel of Fig. 2, we observe that α is constant within systematic
 101 uncertainties, with an average value of 1.207. This average α value is far from the Gaussian assumption

¹ In the conference presentation Minimum Bias data were shown, but here we show and discuss the final 0–30% centrality data of Ref. [13]. The Minimum Bias data are available e.g. in Ref. [27].

102 of $\alpha = 2$ as well as from the conjectured $\alpha = 0.5$ value at the critical point. We show $1/R^2$ as a function
 103 of m_T on the top right panel of Fig. 2. We observe, that the hydro prediction of $1/R^2 \simeq A + Bm_T$ still
 104 holds – even though in hydrodynamics, usually no power-law tails appear, due to the Boltzmann factor
 105 creating an exponential cut-off. This is intriguing point may be investigated in phenomenological
 106 models in the future. The correlation function intercept parameter λ is shown in the bottom left panel
 107 of Fig. 2, after a normalization by

$$\lambda_{\max} = \langle \lambda \rangle_{m_T=0.5-0.7\text{GeV}/c^2}, \quad (14)$$

108 as detailed in Ref. [13]. The m_T dependence of λ / λ_{\max} indicates a decrease at small m_T . This may be
 109 explained by the increase of the resonance pion fraction at low m_T . Such an increase is predicted to
 110 occur in case of an in-medium η' mass, as discussed above. It is interesting to observe that our data are
 111 not incompatible with predictions [28] based on a reduced η' mass, using the Kaneta-Xu model for
 112 ratios of long-lived resonances [29]. Finally, in the bottom right panel of Fig. 2 we show the observation
 113 of a new scaling parameter

$$\hat{R} = \frac{R}{\lambda(1+\alpha)}. \quad (15)$$

114 The inverse of this variable exhibits a clear linear scaling with m_T , and it also has much decreased
 115 statistical uncertainties. Let us conclude by inviting the theory/phenomenology community to
 116 calculate the m_T dependence of the above Lévy parameters, and compare their result to the
 117 measurements.

118 **Acknowledgments:** M. Cs. was supported by the New National Excellence program of the Hungarian Ministry
 119 of Human Capacities, the NKFIH grant FK-123842 and the János Bolyai Research Scholarship.

120 **Conflicts of Interest:** The author declares no conflict of interest.

121 References

1. Adcox, K.; others. Formation of dense partonic matter in relativistic nucleus nucleus collisions at RHIC: Experimental evaluation by the PHENIX collaboration. *Nucl. Phys.* **2005**, *A757*, 184–283, [nucl-ex/0410003].
2. Adams, J.; others. Experimental and theoretical challenges in the search for the quark gluon plasma: The STAR collaboration’s critical assessment of the evidence from RHIC collisions. *Nucl. Phys.* **2005**, *A757*, 102–183, [nucl-ex/0501009].
3. Arsene, I.; others. Quark gluon plasma and color glass condensate at RHIC? The Perspective from the BRAHMS experiment. *Nucl. Phys.* **2005**, *A757*, 1–27, [arXiv:nucl-ex/nucl-ex/0410020].
4. Back, B.B.; others. The PHOBOS perspective on discoveries at RHIC. *Nucl. Phys.* **2005**, *A757*, 28–101, [nucl-ex/0410022].
5. Hanbury Brown, R.; Twiss, R.Q. A Test of a new type of stellar interferometer on Sirius. *Nature* **1956**, *178*, 1046–1048.
6. Goldhaber, G.; Fowler, W.B.; Goldhaber, S.; Hoang, T.F. Pion-pion correlations in antiproton annihilation events. *Phys. Rev. Lett.* **1959**, *3*, 181–183.
7. Goldhaber, G.; Goldhaber, S.; Lee, W.Y.; Pais, A. Influence of Bose-Einstein statistics on the antiproton proton annihilation process. *Phys. Rev.* **1960**, *120*, 300–312.
8. Yano, F.B.; Koonin, S.E. Determining Pion Source Parameters in Relativistic Heavy Ion Collisions. *Phys. Lett.* **1978**, *78B*, 556–559.
9. Adler, S.S.; others. Bose-Einstein correlations of charged pion pairs in Au + Au collisions at $s(\text{NN})^{**}(1/2) = 200\text{-GeV}$. *Phys. Rev. Lett.* **2004**, *93*, 152302, [nucl-ex/0401003].
10. Afanasiev, S.; others. Kaon interferometric probes of space-time evolution in Au+Au collisions at $s(\text{NN})^{**}(1/2) = 200\text{-GeV}$. *Phys. Rev. Lett.* **2009**, *103*, 142301, [arXiv:nucl-ex/0903.4863].

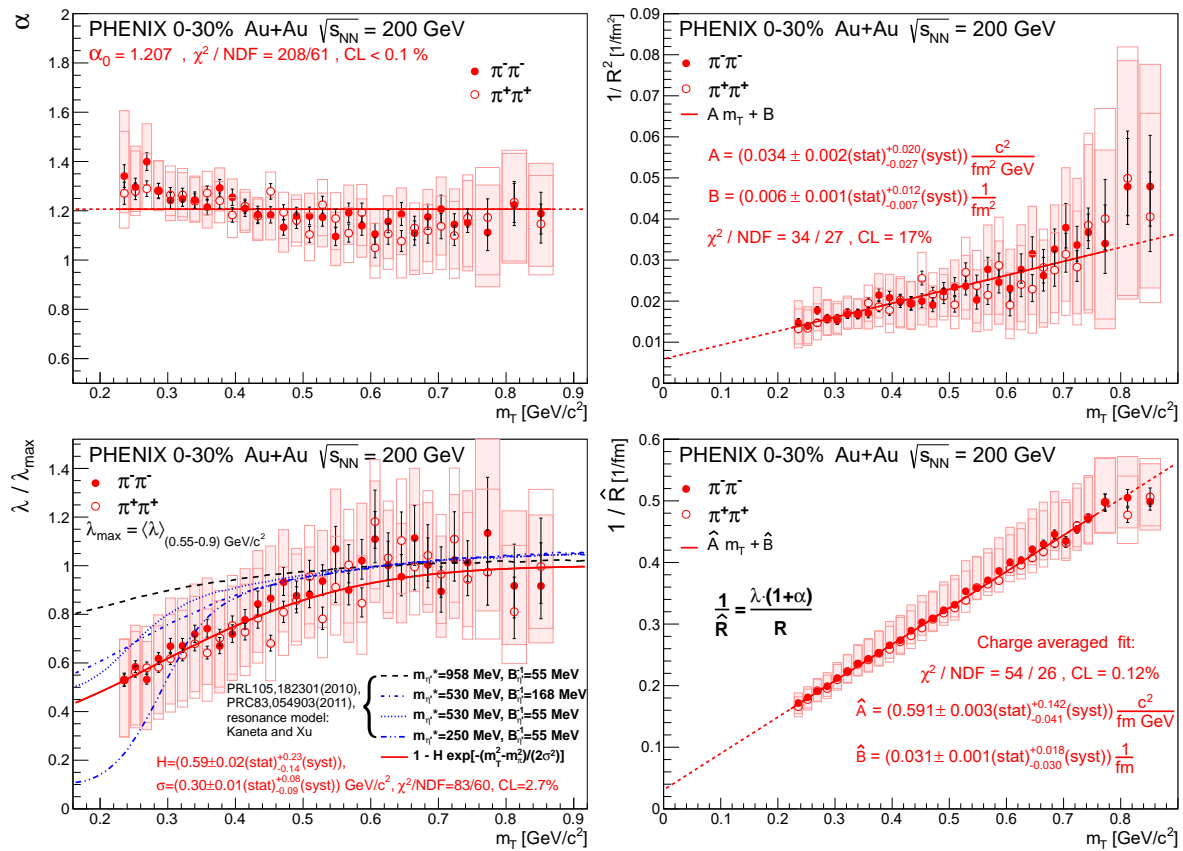


Figure 2. Fit parameters α (top left), R (top right, shown as $1/R^2$), λ (bottom left, shown as λ / λ_{\max}) and \hat{R} versus average m_T of the pair. Statistical and symmetric systematic uncertainties shown as bars and boxes, respectively.

143 11. Makhlin, A.N.; Sinyukov, Y.M. The hydrodynamics of hadron matter under a pion interferometric
144 microscope. *Z. Phys.* **1988**, *C39*, 69.

145 12. Csörgő, T.; Lörstad, B. Bose-Einstein Correlations for Three-Dimensionally Expanding, Cylindrically
146 Symmetric, Finite Systems. *Phys. Rev.* **1996**, *C54*, 1390–1403, [[hep-ph/9509213](#)].

147 13. Adare, A.; others. Lévy-stable two-pion Bose-Einstein correlations in $\sqrt{s_{NN}} = 200$ GeV Au+Au collisions
148 **2017**. [[arXiv:nucl-ex/1709.05649](#)].

149 14. Afanasiev, S.; others. Source breakup dynamics in Au+Au Collisions at $s(\text{NN})^{**}(1/2) = 200$ -GeV via
150 three-dimensional two-pion source imaging. *Phys. Rev. Lett.* **2008**, *100*, 232301, [[arXiv:nucl-ex/0712.4372](#)].

151 15. Adler, S.S.; others. Evidence for a long-range component in the pion emission source in Au + Au collisions
152 at $s(\text{NN})^{**}(1/2) = 200$ -GeV. *Phys. Rev. Lett.* **2007**, *98*, 132301, [[nucl-ex/0605032](#)].

153 16. Metzler, R.; Barkai, E.; Klafter, J. Anomalous Diffusion and Relaxation Close to Thermal Equilibrium: A
154 Fractional Fokker-Planck Equation Approach. *Phys. Rev. Lett.* **1999**, *82*, 3563–3567.

155 17. Csörgő, T.; Hegyi, S.; Zajc, W.A. Bose-Einstein correlations for Levy stable source distributions. *Eur. Phys.
156 J.* **2004**, *C36*, 67–78, [[arXiv:nucl-th/nucl-th/0310042](#)].

157 18. Csanád, M.; Csörgő, T.; Nagy, M. Anomalous diffusion of pions at RHIC. *Braz. J. Phys.* **2007**, *37*, 1002–1013,
158 [[hep-ph/0702032](#)].

159 19. Csörgő, T. Correlation Probes of a QCD Critical Point. *PoS* **2008**, *HIGH-PTLHC08*, 027,
160 [[arXiv:nucl-th/0903.0669](#)].

161 20. El-Showk, S.; Paulos, M.F.; Poland, D.; Rychkov, S.; Simmons-Duffin, D.; Vichi, A. Solving the 3d Ising
162 Model with the Conformal Bootstrap II. c-Minimization and Precise Critical Exponents. *J. Stat. Phys.* **2014**,
163 *157*, 869, [[arXiv:hep-th/1403.4545](#)].

164 21. Rieger, H. Critical behavior of the three-dimensional random-field Ising model: Two-exponent scaling and
165 discontinuous transition. *Phys. Rev. B* **1995**, *52*, 6659–6667.

166 22. Halasz, M.A.; Jackson, A.D.; Shrock, R.E.; Stephanov, M.A.; Verbaarschot, J.J.M. On the phase diagram of
167 QCD. *Phys. Rev.* **1998**, *D58*, 096007, [[hep-ph/9804290](#)].

168 23. Stephanov, M.A.; Rajagopal, K.; Shuryak, E.V. Signatures of the tricritical point in QCD. *Phys. Rev. Lett.*
169 **1998**, *81*, 4816–4819, [[hep-ph/9806219](#)].

170 24. Vance, S.E.; Csörgő, T.; Kharzeev, D. Partial U(A)(1) restoration from Bose-Einstein correlations. *Phys. Rev.
171 Lett.* **1998**, *81*, 2205–2208, [[nucl-th/9802074](#)].

172 25. Kapusta, J.I.; Kharzeev, D.; McLerran, L.D. The Return of the prodigal Goldstone boson. *Phys. Rev.* **1996**,
173 *D53*, 5028–5033, [[hep-ph/9507343](#)].

174 26. Novák, T.; Csörgő, T.; Eggers, H.C.; de Kock, M. Model independent analysis of nearly Lévy correlations.
175 *Acta Phys. Polon. Supp.* **2016**, *9*, 289, [[arXiv:physics.data-an/1604.05513](#)].

176 27. Kincses, D. PHENIX results on Lévy analysis of Bose-Einstein correlation functions. *Acta Phys. Polon. Supp.*
177 **2017**, *10*, 627–632, [[arXiv:nucl-ex/1610.05025](#)].

178 28. Vértesi, R.; Csörgő, T.; Sziklai, J. Significant in-medium η' mass reduction in $\sqrt{s_{NN}} = 200$ GeV
179 Au+Au collisions at the BNL Relativistic Heavy Ion Collider. *Phys. Rev.* **2011**, *C83*, 054903,
180 [[arXiv:nucl-ex/0912.0258](#)].

181 29. Kaneta, M.; Xu, N. Centrality dependence of chemical freeze-out in Au+Au collisions at RHIC (QM2004
182 proceedings) **2004**. [[arXiv:nucl-th/nucl-th/0405068](#)].